The effect of stacking sequence and circumferential ply drop locations on the mechanical response of type IV composite pressure vessels subjected to internal pressure

A numerical and experimental study

Nebe, M.; Johman, A.; Braun, C.; van Campen, J. M.J.F.

DOI
10.1016/j.compstruct.2022.115585

Publication date
2022

Document Version
Final published version

Published in
Composite Structures

Citation (APA)
Nebe, M., Johman, A., Braun, C., & van Campen, J. M. J. F. (2022). The effect of stacking sequence and circumferential ply drop locations on the mechanical response of type IV composite pressure vessels subjected to internal pressure: A numerical and experimental study. *Composite Structures*, *294*, Article 115585. https://doi.org/10.1016/j.compstruct.2022.115585

Composite Structures 294 (2022) 115585

Contents lists available at ScienceDirect

Composite Structures

journal homepage: www.elsevier.com/locate/compstruct

The effect of stacking sequence and circumferential ply drop locations on the mechanical response of type IV composite pressure vessels subjected to internal pressure: A numerical and experimental study

M. Nebe [a,*], A. Johman [a], C. Braun [a], J.M.J.F. van Campen [b]

[a] cellcentric GmbH & Co. KG, Neue Strasse 95, 73230 Kirchheim unter Teck, Germany
[b] Department of Aerospace Structures & Materials, TU Delft, Kluyverweg 1, 2629 HS Delft, The Netherlands

ARTICLE INFO

Keywords:
Composite pressure vessel
Type IV pressure vessel
Pressure vessel
Hydrogen
Hydrogen storage
Fuel cell
Burst experiment
FEA modeling

ABSTRACT

Type IV composite pressure vessels represent the current state-of-the-art for compressed gaseous hydrogen storage in fuel cell electric vehicles. A combination of highly demanding safety regulations and the need for cost competitive solutions make the topic of CPVs particularly challenging. Given the elevated material price of carbon fiber, structural optimality is essential to meet both requirements. Thorough understanding of design parameters and mechanical performance of composite pressure vessels is prerequisite to structural optimality. In this paper we investigate the relation of stacking sequence and circumferential ply drop locations on the mechanical performance of type IV composite pressure vessels subjected with internal pressure. This paper builds on previous studies by the authors, which are enhanced by new numerical and experimental results. An experimental set is used, where for a given layup composition the stacking sequence and the circumferential ply drop locations are varied. The experimental results are complemented by a computationally efficient numerical framework, which is composed by the output of a commercial filament winding software, a self-developed geometry correction algorithm and an automated FE model generation program. The numerical results are compared with outer surface strains obtained by means of three-dimensional digital image correlation, the final burst pressures and the vessel remainders. The achieved burst pressures vary between 152.6 and 188.6 MPa, depending on design configuration. For the layup composition in this investigation, the placement of tangentially reinforcing layers (e.g. circumferential and high-angle helical layers) as innermost layers led to overall higher cylinder strengths compared to sequences, where these layers were located as outermost. The retraction of circumferential ply drop locations was found to impact the burst performance differently in dependence of the stacking sequence. For sequences, where circumferential layers were located as outermost, a retraction of ply drop locations by 12 mm showed barely any differences in burst pressure (-1.9%). For sequences, where these layers were located as innermost, a severe decrease (-19.1%) was noticed once the ply drop locations were retracted by up to 9 mm. The results not only underlined the criticality of both design parameters and their interaction with each other, but also showcased a computationally efficient numerical framework capable of capturing distinct mechanical responses for a variety of layups at least trend-wise.

1. Introduction

The electrification in each segment of today's mobility is a necessity to minimize the impact of transportation on greenhouse gas emissions. Particularly for long haul transportation, the use of hydrogen powered fuel cells appears as a promising solution. A crucial part of a fuel cell electric vehicle (FCEV) is its hydrogen storage system. Currently, hydrogen is most often stored in a compressed gaseous state in type IV pressure vessels, which are made of a polymer liner and a carbon fiber-reinforced plastic (CFRP) overwrap [1–3]. Given the high nominal working pressures of 35 or 70 MPa, the vessels need to be designed to meet highest safety standards. At the same time, the high raw material price of carbon fiber leads to the fact, that an optimized material usage is required to be cost competitive. To enable further cost savings, the mechanical response of composite pressure vessels (CPVs) under internal pressure loading needs to be studied thoroughly.

Studying the mechanical response of CPVs is a sophisticated task, because of the complexity that is introduced by the stacking multiple layers of CFRP. In previous studies experimental and numerical efforts

* Corresponding author.
E-mail address: martin.nebe@cellcentric.net (M. Nebe).

https://doi.org/10.1016/j.compstruct.2022.115585
Received 31 December 2021; Received in revised form 5 April 2022; Accepted 8 April 2022
Available online 29 April 2022

were made to gain insights into the mechanical response of CPVs under internal pressure loading. Experimental work featured the characterization by means of acoustic emission (AE) [4–6], electrical resistance strain gauges (ESGs) [7–9], linear variable differential transformers (LVDTs) [2,10], fiber optic sensors (FOSs) [11,12] and digital image correlation (DIC) [13–15].

Likewise efforts related to numerical modeling can be differentiated by certain aspects, such as used element types, the implementation of damage progression and the considered scale of material. Model approaches entailed the use of axisymmetric shells [2,10,16] and three-dimensional solid elements [2,10,16–18]. Furthermore, numerous approaches considered constitutively elastic solutions [19,20], while others implemented continuum damage mechanics (CDM) models [2,18,21] to account for the material degradation that takes place during the internal pressure loading. Concerning the material scale, the majority of works related to CPVs focuses on mesoscale base while few even consider the microscale [22,23]. A defining aspect of most previous numerical work is the high computational cost of developed models. Most rely on a per-ply modeling approach in order to try and capture as much of the underlying mechanics as possible since the significance of most mechanical particularities for CPV performance is not entirely understood. We also recently presented a model applying a per-ply modeling approach in [15], which further considered the material degradation during internal pressure loading through the CDM subroutine *Compdam* [24]. While the high level of detail in these simulation models allows for an in-depth analysis of selected vessel configurations, it is difficult to transfer these modeling strategies to an industrial environment due to the implied high computational costs.

Even though each numerical method and experimental characterization technique contributes to a better understanding of the mechanical response of CPVs under internal pressure loading, little is known about the impact and the interaction of design critical aspects of CPVs. For example, it is known that the choice of stacking sequence impacts multiple aspects like stress–strain distribution through-the-thickness, initiation and propagation of interfiber failure as well as laminate consolidation, but to which extent and what this means for the final burst strength is yet unclear. Also, it is known that the ply drop locations of circumferential layers impact the stress–strain distribution in the cylinder–dome transition region but how much it influences the deformation behavior as well as the burst pressure is not known. Finally, the question arises whether the choice of stacking sequence and circumferential ply drop locations impact each other too.

With this paper, we are aiming to shed light on the influence of stacking sequence and circumferential ply drop locations on the mechanical response of CPVs subjected to internal pressure. The two variables are investigated individually and their interaction with each other is explored too. The impact is quantified in terms of deformation behavior and final burst pressure. This is done by comparing numerical and experimental results for a total of six vessel configurations and twelve vessels in total. The vessels are pre-designed, manufactured and tested within the same facility. While the experimental setup shown in this investigation already has been subject to previous publications [14,15], this work also showcases a novel and computationally efficient numerical modeling approach that can be applied to a variety of layups in future.

2. Previous research

This paper builds upon work published by Nebe et al. [14] and Nebe [25]. In [14], the influence of stacking sequence on the CPVs mechanical response was assessed by comparing analytical and experimental results. For the sequences shown in Fig. 1, the outer strains and the maximum strength of the cylindrical section were determined by using a three-dimensional elasticity approach developed by Xia et al. [26] and compared to experimental outer strains obtained by means of digital image correlation (DIC) as well as the final burst pressures. Subsequently, in [25] numerical results and further experimental data were added to analyze the reasons for the effects encountered in the prior investigations of [14]. In the following, the results of the prior investigations with regard to two aspects are discussed here, the cylinder deformation trends and the cylinder–dome deformation trends.

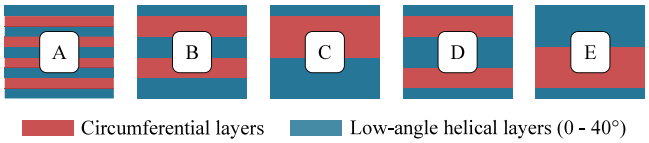

Fig. 1. Investigated sequences by Nebe et al. [14].

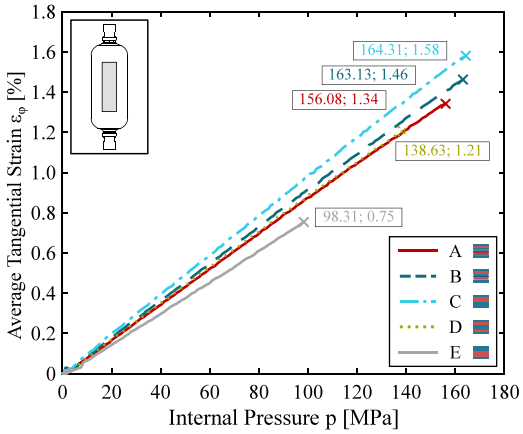

Fig. 2. Comparison of tangential cylinder strains of different stacking sequences. *Source:* Adapted from Nebe et al. [14].

2.1. Cylinder deformation trends

The change of through-the-thickness stiffness distribution by the different placement of circumferential layers naturally impacts the stress–strain distribution in the CPV's wall. In [14] the impact of the different circumferential layer placement was particularly noticeable in the tangential expansion of the CPV's cylindrical section as Fig. 2 shows.

The differences in tangential cylinder expansion between the sequences are readily explained by the through-the-thickness load distribution and the location of the most tangentially stiff layers in the laminate—circumferential layers. Placing circumferential layers as innermost layers of a stacking sequence more directly exposes them to the tangential loads, which are highest on the inside. This in turn, restricts the tangential expansion relative to cases where circumferential layers are placed as outermost layers of a stacking sequence. In the latter case, the tangentially more compliant layers, such as low-angle helical layers, placed as innermost layers are required to transfer these tangential loads to the load carrying circumferential layers on the outside. This results in a larger tangential expansion in the cylinder. This effect is most clearly visible within the comparison of the distinct Sequences E and C in Fig. 2 where, at 70 MPa internal pressure, the tangential strain in Sequence E was presented to be nearly 20% lower than in Sequence C.

2.2. Cylinder–dome deformation trends

Besides the differences in tangential cylinder expansion, the strain distributions in the cylinder–dome transition region also showed different trends in the work of Nebe et al. [14]. While for the Sequence C comparably low tangential strains were seen, for Sequence E a large

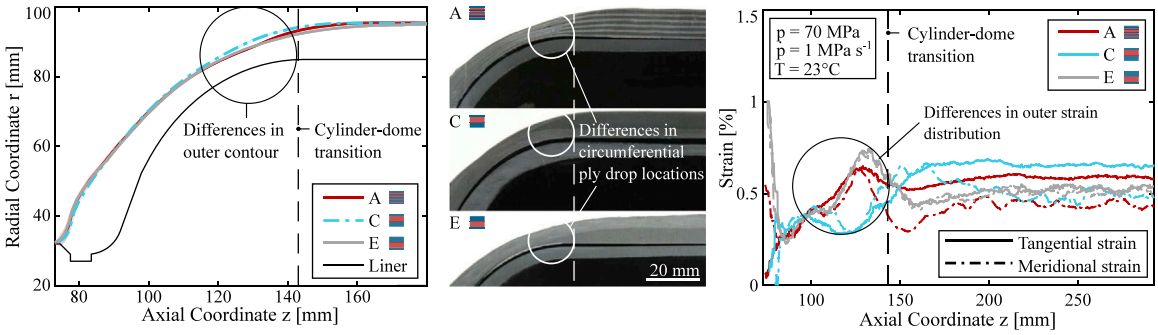

a) Experimental thickness profiles b) Cross-sections cylinder-dome transition c) Strain distribution cylinder-dome transition

Fig. 3. (a) Experimental thickness profiles obtained by means of outer contour scans, (b) cross-sectional view on circumferential ply drop locations and (c) strain distribution in the cylinder–dome transition region.
Source: Adapted from [14,25].

tangential expansion was recognized. Next to that, the Sequence E showed a preliminary failure outside the cylindrical section. Further investigations revealed the development of interlaminar damage by means of a delamination between the layer groups of circumferential and low-angle helical layers in the cylinder–dome transition region. This may or may not have been a result of the large deformations encountered in this region. By the time writing, possible explanations for the distinct behaviors entailed the ply drop locations of circumferential layers as well as the influence of extensional–bending coupling due to the stacking sequence asymmetry. Yet, given the limited data a clear distinction of these effects was not possible.

Nebe [25] further detailed these investigations by obtaining outer contour scans, cross-sections of the cylinder–dome transition regions and strain distributions along the meridional surface path of the vessels. An excerpt of these results is shown in Fig. 3.

It is necessary to interpret the combination of results shown in Figs. 2 and 3 in order to shed light on the discussion that follows later in this work. The measured outer contours in Fig. 3 (a), which were obtained by means of stripelight projection, indicated a slight difference in geometry between the Sequences A,C and E in the area of the cylinder–dome transition region. The change in geometry at the transition appeared to be a result of the manufacturing of these vessels. Even though the nominal circumferential ply drop locations were kept identical between the configurations, the different stacking of circumferential and low-angle helical layers caused variations in how far the circumferential ply drop locations would extend in the dome. This difference is visible in the vessel cross-sections seen in Fig. 3 (b). For Sequence C the circumferential ply drop locations would extend the farthest into the dome, which is accompanied by the lowest strains encountered in the cylinder–dome transition zone, seen in 3 (c). In contrast to that, Sequence E would show the most retracted circumferential ply drop locations and the highest strains in the cylinder–dome transition region. Given these observations, the strain distribution in the cylinder–dome transition appeared to be not only influenced by the different stacking sequences, but also by the extent to which the circumferential ply drop locations would reach into the dome. Retracted circumferential ply drops would manifest itself in a local decrease in tangential stiffness leading to high strains, while extended ply drops would ensure sufficient local tangential stiffness and correspondingly low strains. This effect was particularly present for the investigated sequences in [14,25] due to the chosen layup composition. Given the fact, that the sequences were composed by mainly two layer types, circumferential and low-angle helical layers, the tangential stiffness distribution in the cylinder–dome transition was particularly dependent on the ply drop locations of the circumferential layers.

Altogether, the multitude of effects present in previous investigations [14,25] motivated the investigation of the two relevant design criteria in this research, namely stacking sequence and the locations of circumferential ply drops.

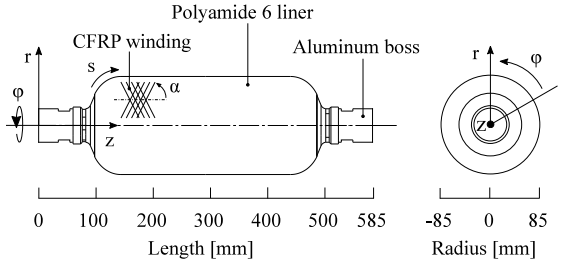

Fig. 4. Subscale geometry under investigation.

3. Materials

3.1. Material

The material that we used for filament winding is a towpreg composed of an epoxy resin reinforced with high-strength carbon fibers. The material is identical to the material used in previous works and was experimentally characterized by Nebe et al. [15,25] through the testing of unidirectional and interwoven bidirectional flat filament wound coupons accompanied by fiber volume fraction and porosity measurements. Table 1 shows a summary of the tensile and shear properties.

3.2. Subscale vessel geometry

For all specimens the liner-boss assembly geometry, depicted in Fig. 4, was used. The mandrel itself consists of a polyamide 6 shell with two aluminum boss ends. The internal volume of the mandrel is 8.6×10^{-3} m^3. The indicated coordinate system in Fig. 4 is identical to previous works [14,15,25], where s designates the meridional coordinate, φ indicates the tangential coordinate and z represents the axial coordinate.

3.3. Experimental design

Resulting from the previous research [14,25], two main variables are investigated in this work. The experimental design is shown in Fig. 5. The influence of the stacking sequence is assessed by considering two distinct sequences named BL and BC, seen in Fig. 5 (a). These sequences closely resemble the Sequences C and E in [14,25] with the main difference being the addition of high-angle helical layers to reduce the criticality of stiffness variations in the cylinder–dome transition region.

The influence of circumferential ply drop locations is evaluated by creating additional variants of the Sequences BL and BC with

Table 1
Experimentally determined tensile and shear properties [27,28] with indicated fiber volume fractions and porosities [29] from Nebe et al. [15]; values depict average ± standard deviation.

Laminate	E [GPa][1]	σ_{max} [MPa][1]	ε_{max} [%][1]	V_f [%][2]	V_p [%][2]
0°	127.28 ± 1.30	2369.30 ± 53.77	1.63 ± 0.07	57.16 ± 0.13	3.19 ± 0.10
90°	7.63 ± 0.02	29.90 ± 1.38	0.40 ± 0.02	57.88 ± 0.38	2.74 ± 0.19
Laminate	G [GPa][1]	τ_{max} [MPa][1]	$\tau_{5\%}$ [MPa][1]	V_f [%][2]	V_p [%][2]
±45° $_{iw}$	3.85 ± 0.07	55.34 ± 5.56	49.56 ± 2.02	60.17 ± 2.47	3.65 ± 1.02

ν_{12}[1] = 0.34 ± 0.02 E - normal elastic modulus; σ_{max} – maximum normal stress; ε_{max} – strain at maximum normal stress; G – shear elastic modulus; τ_{max} – maximum shear stress; $\tau_{5\%}$ – shear stress at 5% strain; V_f - fiber volume fraction; V_p – void volume fraction or porosity; ν_{12} – Poisson's ratio; $_{iw}$ – interwoven[1] min. 8 samples tested per configuration; [2] 5 samples tested per configuration.

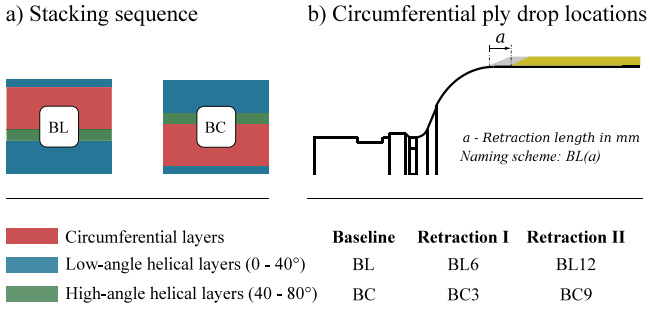

Fig. 5. Two investigated variables within the experimental design.

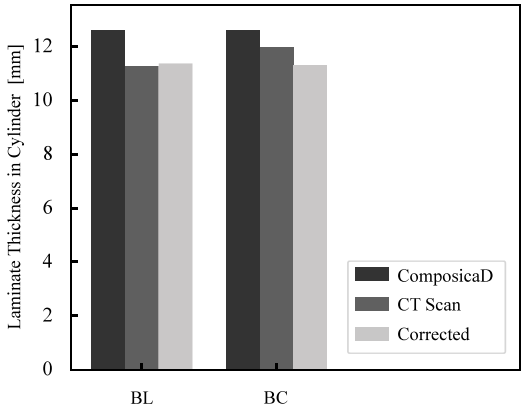

Fig. 6. Comparison of *ComposicaD*, CT scan and corrected laminate thicknesses in the cylinder for stacking sequences BL and BC.

different ply drop locations. Per sequence, two variants are generated by retracting the circumferential ply drop locations by the length a. It is important to mention that the length a represents the nominal retraction in the filament winding program, not the final location after winding and curing. The variation in circumferential ply drop location is represented by the Sequences BL6, BL12 and BC3, BC9. The different retraction for the BC and BL series is a manufacturing-related consideration. For the Sequences BL, BL12 and BC3 three vessels are manufactured and tested, whereas for the Sequences BC, BC9 and BL6 only one vessel is considered.

4. Methods

4.1. Numerical modeling approach

The modeling approach used in this work was developed in context of the industrial application. Besides highly detailed and numerically expensive FE models, that serve the purpose of pinpointing specific phenomena in selected CPV designs, it is important to identify certain trends in deformation behavior and burst performance to a reasonable degree of accuracy in early stages of the design phase. The modeling approach presented in this work was created with this principle in mind. Therefore, all major aspects of the approach were automated and are valid for any arbitrary layup configuration using the same liner geometry. Fig. 7 illustrates the substeps of the approach.

Initially, a vessel layup is defined through the filament winding software *ComposicaD* [30]. The software not only allows to derive machine motions, but also permits to retrieve information about the variation of angle and thickness for each ply. However, the data generated by *ComposicaD* does not take into account the layer interactions during winding and curing, resulting in unrealistic thickness predictions. To adjust for this result, an automated, ad-hoc, thickness correction algorithm was developed that combines aspects of an analytical model and a set of specially developed non-dimensional correction factors that were used to adjust layer placement and mimic observed layer behavior during winding. The output of the thickness correction algorithm is then fed into a parametrized *ABAQUS* model which automatically generates the vessel geometry, boundary conditions, load distributions etc. Lastly, the results of the *ABAQUS* model are post-processed to present strain and stress data as well as provide an approximation of burst pressure.

The geometry correction algorithm tackles the vessel's geometry correction through a three-fold approach wherein three types of layers are identified that require slightly different corrections—circumferential layers, high-angle helical layers, low-angle helical layers. Fig. 8 shows a graphical summary of the differences between representative *ComposicaD* output and corrected output. To generate the shown geometry correction, a set of non-dimensional factors were developed to mimic the observed behavior of layer movement during winding. The tapering region of circumferential layers was given most focus during the development of these factors since the cylinder–dome transition was the focal point of the experimental set. A detailed overview of the non-dimensional parameters can be found in [31].

The thickness correction aspect of the geometry correction was made by applying a physical model of thickness variation in wound cylinder as presented by Kang et al. [32]. The model takes developed Lamé equations for orthotropic cylinders to derive the stress state per-layer in a wound cylinder. The stress-state of plies can then be converted into strain and compaction for geometry correction. The model was extended to also be used in the domes of the CPVs analyzed. To do this, the domes were treated as consecutive, concentric cylinders. Fig. 6 shows the predicted change in laminate thicknesses in the cylinder for stacking sequences BL and BC.

The solution briefly described is of a purely engineering nature—meaning it would likely require significant alterations for application to a manufacturing process to the one at cellcentric GmbH & Co. KG. Regardless, the solution was observed to provide reasonable results for the outer contours of all configurations tested both by Nebe et al. [14] and in the configurations tested in this study.

4.2. FE model definition

The application of the workflow shown in Fig. 7 enables the consistent generation of CPV geometries with a smooth upper and bottom

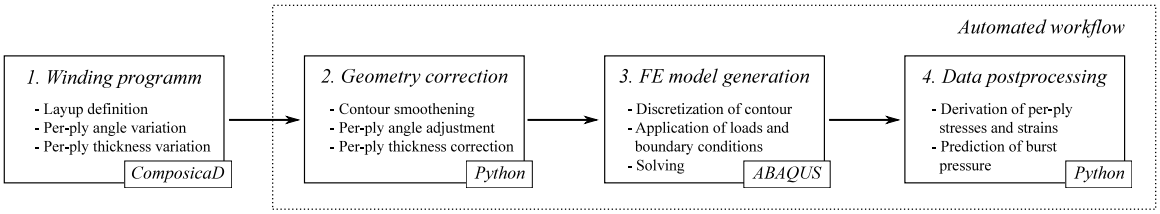

Fig. 7. Individual steps of the FE modeling approach used for time-efficient CPV analysis.

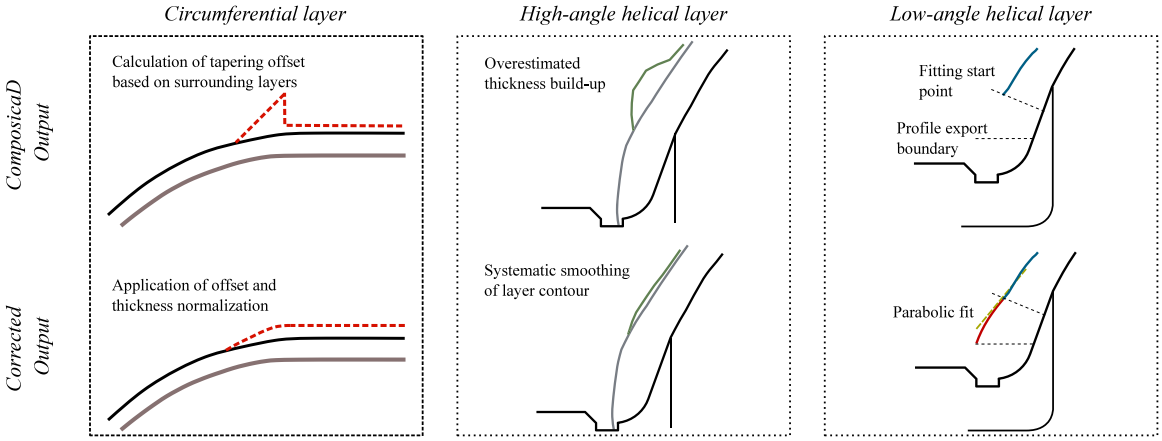

Fig. 8. Schematic summary of layer distribution correction per layer type.

contour—implying a plausible distribution of layers in the cylinder–dome transition region. Using the top and bottom contour, a single solid part is generated in *ABAQUS* to describe the vessel's geometry. The solid part is then partitioned longitudinally and through-the-thickness. Each section is assigned a single stacking sequence where layer thickness is determined by the thickness correction algorithm. In the model's presented form, the solid part is only partitioned through-the-thickness once. The through-the-thickness partition was found to be necessary due to the large number of sections in the longitudinal direction of the CPV which caused very high aspect ratios on some elements. While the presented partitioning strategy still produces high aspect ratios, the performance of the model was observed to be consistent between tested configurations. Nevertheless, exploring different partitioning strategies is a topic of interest for future studies since the regularity of element aspect ratios is likely to affect results.

Fig. 9 shows the three-dimensional depiction of the vessel model. The model describes 1/8th of the subscale geometry described in Section 3.2. Since previous studies [2,15,16] demonstrated the importance of through-the-thickness normal stress gradients in the prediction of constitutively elastic mechanical response, the model utilizes the quadratic formulation of *ABAQUS*'s solid elements—C3D20R. The use of a quadratic element formulation was found to be beneficial since it was a fairly straightforward method to effectively reduce high aspect ratios through-the-thickness. The use of continuum shell elements was initially considered but not followed since the coupling of the out-of-plane radial stress and the in-plane normal stresses (longitudinal, transverse) was deemed essential because of the large wall thickness. Due to its low rigidity in comparison to the CFRP overwrapping, the polyamide 6 liner was not considered in the FE model.

The material properties used in the numerical model are summarized in Table 2. The properties defined in Table 2 are the same as used in [15]. The determination of these properties resulting from the experimental test data in Table 1 is further explained in [15]. Using the same material properties allows for performance comparison and highlights the importance of through-the-thickness partitioning in numerical modeling of CPVs.

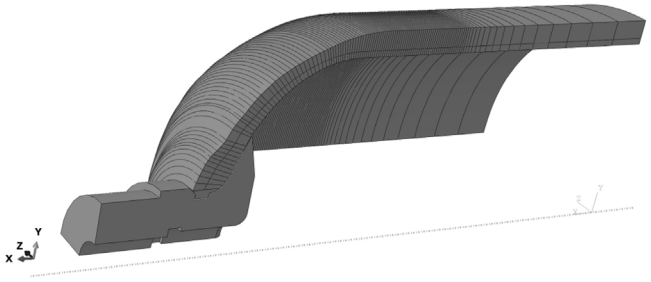

Fig. 9. FE discretization of the numerical model developed for time-efficient CPV analysis.

Table 2
Composite and resin properties defined in FE model.

Composite Reinforcement
Elastic Properties
E_{11} = 135.65 GPa; E_{22} = 8.03 GPa; $G_{12,iw}$ = 3.85 GPa;
ν_{12} = 0.34; ν_{23} = 0.34
Ply Strengths
X^T = 2524.20 MPa; Y^T = 31.47 MPa;
Y^C = 225.80 MPa; S^L_{iw} = 49.56 MPa;

While the main purpose of the numerical model developed for this paper was to evaluate the ability of the described model to depict the different structural response relative to the CPV layup variation, burst pressure remained a useful metric by which to gauge the limitations of the developed model. Therefore, a first-ply-failure approach was implemented into the post-processing of model data.

Puck failure criterion, shown in Eq. (1), was used to provide a baseline approximation for first-ply-failure analysis since its definition takes into account both the in-plane and out-of-plane stress state of the material.

$$\frac{1}{\pm X_{T,C}}\left[\sigma_{11}-\left(\nu_{21}-\nu_{21,f}m_{\sigma f}\frac{E_{11}}{E_{11,f}}\right)(\sigma_{22}+\sigma_{33})\right]=1 \tag{1}$$

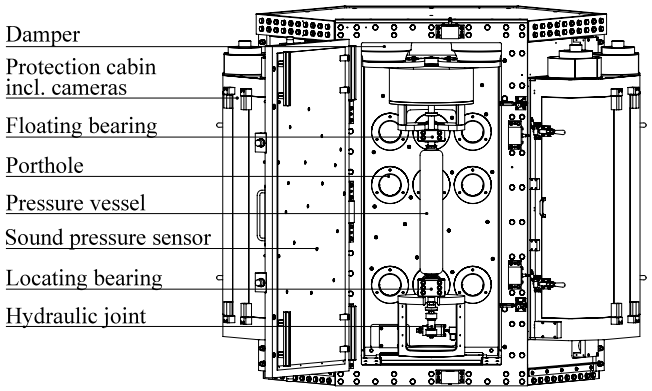

Fig. 10. Test chamber for burst and cyclic experiments of pressure vessels.

Where $X_{T,C}$ is longitudinal tensile or compressive strength, ν_{21} is Poisson ratio in the longitudinal direction due to transverse loading, E_{11} is Young's modulus in the longitudinal direction and $E_{11,f}$ refers to fiber Young's modulus. $m_{\sigma f}$ is an arbitrary factor that proposed to be 1.1 for CFRP.

To predict burst, only the fiber failure mode was used in this study, which neglects the initiation and progression of interfiber failure. A limitation in using Puck failure criterion is in its inability to account for shear stresses when predicting damage occurrence. In all configurations, significant shear stresses are likely to develop between circumferential and helical layer interfaces.

Lastly, it should be pointed out that the purpose of the presented model was not to accurately demonstrate the damage evolution process within the laminate but to showcase a computationally efficient modeling framework, that is capable of reproducing different deformational trends. The use of damage progression subroutines for an accurate burst pressure prediction has been shown by other authors [2,15,33] in the past and poses an interesting topic for the future implementation into this modeling framework.

4.3. Experimental setup

The experimental work is carried out in a specially designed test chamber, shown in Fig. 10, where vessels are hydraulically pressurized until burst. The chamber has been utilized in prior investigations [14,15,25]. Through a locating–floating bearing scheme, the vessels are clamped inside the chamber. This allows for axial and radial expansion during the pressurization. A hydraulic joint located below the locating bearing enables the pressurization with a rate of $1\,\mathrm{MPa\,s^{-1}}$.

The chamber features two measurement systems. An array of 120 sound pressure sensors for the recording of airborne acoustic emissions as well as nine stereometric systems, composed by two cameras and one projector each, for obtaining the outer contour and the outer strain during pressurization. The strain measurement, which is the main focus of this work, is performed by means of DIC. The camera resolution is $1624 \times 1234\,\mathrm{px}$ and the frame rate is $1\,\mathrm{Hz}$. For postprocessing the software *GOM Correlate Professional* (GOM, Braunschweig, Germany) is used. The postprocessing methodology to retrieve strain information from the multisensor system is explained in [14,15,25] and is therefore not further detailed in this work.

5. Results and discussion

The following section is assembled to first assess the two investigated variables, variation of stacking sequence and circumferential ply drop locations, separately. Therefore, results from the experimental set as well as from the numerical modeling approach are reviewed. Lastly, by evaluating the interaction between both variables, insights related to the design of CPVs are derived.

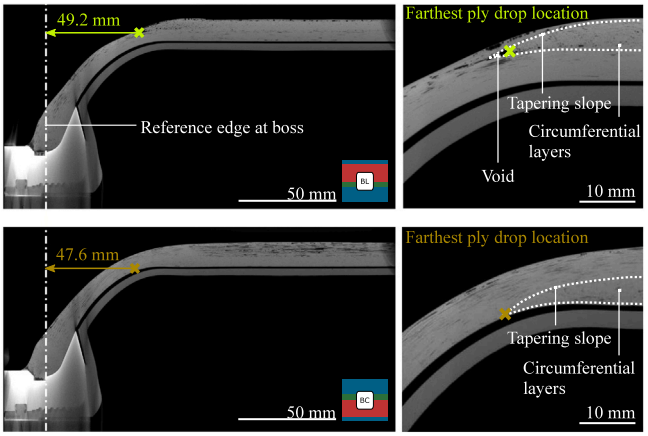

Fig. 11. CT scan of one specimen for Sequences BL and BC; the farthest circumferential ply drop location was determined by manually measuring its distance to a reference edge at the metall boss.

5.1. Variation of stacking sequence

The influence of stacking sequence is investigated by comparing the sequences BL and BC. The two sequences are selected to minimize the impact of varying circumferential ply drop locations. During the manufacturing, attention was paid to ensure similar circumferential ply drop locations. However, when virtually having identical ply drop locations in the winding program, the distinct layer sequences not only cause a different redistribution of material during the winding and curing, but also impact the shrinkage of the liner, which in turn also affects the circumferential ply drop locations in the cylinder–dome transition region. Therefore, the farthest ply drop locations were modified to account for these differences and to achieve similar circumferential ply drop locations. To evaluate this, CT scans were performed and the position of the farthest circumferential ply drop was measured. Fig. 11 shows the comparison between Sequence BL and BC, where still a slight difference of $1.6\,\mathrm{mm}$ in the farthest circumferential ply drop location is recognized. Due to limited resources, only these two Sequences (BL and BC) were CT scanned. The vessels were considered as they further highlight the differences in tapering slope as a result of stacking sequence. The exact layer placement cannot be guaranteed for the other Sequences due to the potential for layer rearrangement during and after winding, but great attention was given to minimize any manufacturing influence that could potentially impact the placement.

It is worthwhile to mention that besides the differences in the farthest circumferential ply drop location, the slope at which the stack of circumferential layers tapers off is also different. Based on observations during the manufacturing of these vessels, the position of the circumferential stack through-the-thickness as well as the number of helical layers wound above the stack appear to determine the slope at which the circumferential layers are tapered off. While the position of farthest circumferential ply drop location was adjusted in the winding program, the tapering slope was not. Between the Sequences BL and BC, the nominal tapering length in the winding program was kept the same. Any changes in the slope are the sole influence of the stacking sequence, that shall be considered when evaluating the results.

Impact on the cylinder deformation

The change in stacking sequence between the configurations of BL and BC inherently promotes different distributions of stress and strain through the vessel's wall. Depending on whether tangentially reinforcing layers, like circumferential or high-angle helical layers, are located as inner or outer layers, the tangential expansion of the cylinder varies. Fig. 12 shows outer meridional and tangential strains along the meridional surface path for both sequences. In the case of Sequence BL,

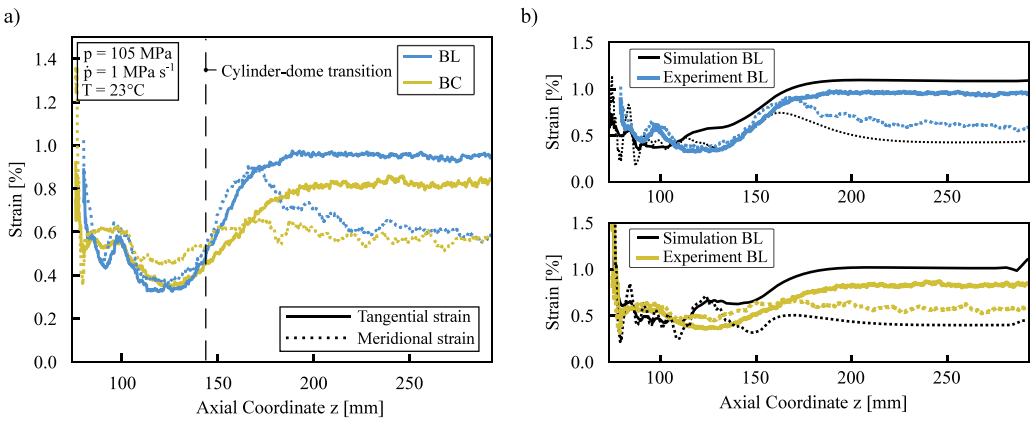

Fig. 12. Influence of the stacking sequence on the outer surface meridional and tangential strains; (a) Experimental strains for Sequences BL and BC; (b) comparison of predicted and experimental strains along the meridional surface path.

where high-angle helical and circumferential layers are located further on the outside, the vessel cylinder is expanding more, as the high tangential loads need to be transferred from the compliant low-angle helical layers on the inside to the high-angle helical and circumferential layers on the outside. This is perceived by a tangential strain of about 1% in the cylindrical section at 105 MPa of internal pressure. Contrarily, for Sequence BC, where high-angle helical and circumferential layers are positioned on the laminate inside, a much lower tangential cylinder expansion is perceived. At the same pressure level, the cylindrical section is showing a tangential strain of 0.8%.

The distinct tangential cylinder expansion is also likely to cause differences in the initiation and progression of matrix damage. The load transfer through the low-angle helical layers to the outer positioned high-angle helical and circumferential layers for Sequence BL is expected to yield in the development of interfiber fracture in the low-angle helical layers, which in turn increases the compliance in the tangential direction. In contrast, the inner positioned high-angle and circumferential layers carry the loads directly, which not only reduces the tangential expansion, but also the degree to which interfiber fracture is initiated in the low-angle helical layers.

Apart from the observations on the tangential strain, the meridional strains in the cylindrical section are almost the same for both sequences, reaching values around 0.6% at an internal pressure of 105 MPa. This resides in the fact that contrarily to the tangential loads, the dome-to-dome transferred meridional loads do not feature a gradient through-the-thickness, which reduces the significance of the stacking sequence to the meridional strain component.

Impact on the strain distribution in the cylinder–dome transition

The changes in tangential cylinder expansion further impact the existence and magnitude of meridional bending in the cylinder–dome transition zone. Based upon the individual expansion of cylinder and dome, meridional bending is recognized by a change in outer meridional strain along the surface. Considering a similar deformation in the dome, meridional bending is increased for the configuration that expands tangentially more in the cylinder. This is the case for the Sequence BL. Here, the outer meridional strain component increases at the cylinder end, which indicates an inward bending cylinder due to the rigid connection to the dome. For the Sequence BC also an inward bending cylinder is recognized, even though the magnitude at which the meridional strain is increasing towards the transition is much smaller, which is a result of the lower tangential cylinder expansion. Additionally, the response at the transition from cylinder to dome is not only impacted by the bending stiffness of the laminate, but also by its extensional–bending coupling response in the meridional direction. In case of the latter, two vastly distinct responses are expected for the Sequences BL and BC. Nonetheless, the multitude of effects arising at the cylinder–dome transition hinder to confidently determine the impact of this aspect.

Fig. 12 (b) shows the comparison of predicted and experimental strains. The deformation behavior, particularly the response at the cylinder–dome transition region, is well resembled by the FE model for both sequences. Nonetheless, certain differences in strain magnitude are observed. While tangential strains are always overestimated, meridional strains are constantly underestimated. These discrepancies are anticipated due to certain limitations of the FE modeling approach, that are mentioned at this point.

Firstly, the thickness correction approach by Kang et al. [32] used in this work refines the wall thickness based upon the consideration of winding stresses (the consideration of curing related stresses was neglected in this work due to missing material properties). The thickness was adjusted without further correction for local fiber volume fractions. By compacting a laminate, a decrease in ply thickness and an increase in fiber volume fraction is expected. Refining the thickness without increasing the fiber volume fraction, effectively removes composite material in the FE model. This in turn increases the predicted compliance and leads to an overestimation of strains, which is more noticeable in the tangential direction because the relative compaction the high-angle helical and circumferential layers is higher than it is in the low-angle helical layers.

Secondly, the presented modeling approach neglects the existence of damage. As seen in prior work by Nebe et al. [15], interfiber failure initiates due to transverse tension in both, helical and circumferential layers. In dependence of the layup composition, the impact of this interfiber failure on the meridional and tangential strain component can be different. For a layup that has a representative number of circumferential layers, that majorly control the deformation behavior in the tangential direction, the impact of interfiber failure on the tangential strain is comparably low. Contrarily, for the meridional strain component, where low-angle and high-angle helical layers are aligned in an angle to the meridional loading direction, the impact of interfiber failure can be noticeably higher. At an internal pressure of 105 MPa, interfiber failure developed throughout the vessel laminate, which particularly increased the compliance in the meridional direction. As in the FE model the existence of damage is neglected, meridional strains appear to be generally underestimated compared to the experiment.

While in cylinder and cylinder–dome transition region the deformation behavior is relatively well depicted, a few numerical irregularities are noticed in the dome region. Particularly the depiction of helical layer angle variation and thickness distribution around their polar openings cause numerical inaccuracies that are appreciated as rapid changes in local strains as well as stresses. For further refinement, a physical sound model is required that considers the changes in angle, fiber volume fraction and thickness for a given axial coordinate within

Fig. 13. Vessel remainder of the two investigated Sequences BL and BC.

the dome region. As this work is mainly dealing with effects related to the cylinder and cylinder–dome transition, this region is not further evaluated here.

Impact on the failure mode and burst pressure

The impact of the stacking sequence on the final failure is investigated by observing the vessel remainders after failure and by comparing the predicted and experimental burst pressures. Fig. 13 shows the remainders of one vessel for the Sequences BL and BC as well as the experimentally obtained burst pressures. Even though a certain ambiguity always exists when evaluating vessel remainders, for both sequences a cylinder failure is concluded as partial sections of both dome ends are still attached to the metall bosses. While the failure location appears to be similar for both sequences, differences in the obtained burst pressures are noticed. The Sequence BC shows a noticeably higher burst pressure of 188.7 MPa compared to the Sequence BL, where an average burst pressure of 163.3 ± 1.3 MPa has been determined.

As for both sequences the cylinder appeared to be the failure determining region (which was the intended target for this investigation), the following discussion is specifically aimed towards the effects of stacking sequence on the cylindrical section. The obtained differences in burst pressure are expected to be the result of two major influences, the distribution of fiber volume fraction through-the-thickness and the progression of damage.

In previous research by Nebe et al. [14] it became apparent that the stacking sequence noticeably impacts the distribution of fiber volume fraction and porosity through-the-thickness. In the cylindrical section high-angle layers (high-angle helical or circumferential layers) apply higher compaction towards previously wound layers than low-angle helical layers do. In the case of Sequence BL, it is expected that the low-angle and high-angle helical layers exhibit a high consolidation level due to their position as inner layers. The outer positioned circumferential layers apply a noticeable compaction towards these layers but most likely show a lower consolidation level than the circumferential layers in Sequence BC, where they are located as inner layers. For Sequence BC, the highest compaction is expected in the circumferential layers, because of the compaction that is being applied through the high-angle helical layers. The low-angle helical layers in Sequence BC show a very low consolidation level in the cylindrical section, as they do not receive further compaction on the laminate outside. This increased porosity in the outer layers of Sequence BC is also visible in the CT scans in Fig. 11.

Table 3
Overview of predicted and experimental burst pressures.

Stacking sequence	Number of vessels	Burst pressure [MPa]		Relative difference
		Experiment	Simulation	
BL	3	163.3 ± 1.3	161.8	−0.9%
BC	1	188.7	155.2	−17.7%

While differences in the local distribution of fiber volume fraction are present, the question arises about whether one or the other layer consolidation level is more important for the cylinder strength of the vessel than others. Generally, high-angle helical and circumferential layers highly contribute to the cylinder strength as they carry the governing tangential loads. In that sense, a higher consolidation level in these layers is anticipated of higher importance than for example in the low-angle helical layers. Therefore, one could advocate for Sequence BC, where the cylinder-strength contributing circumferential layers are likely of higher consolidation than they are found in the Sequence BC.

On the other hand, the cylinder expansion alongside with the progression of damage is deemed to be one of the critical reasons for the difference in burst pressure between Sequences BL and BC. As previously mentioned, the stacking sequence of BL requires the high tangential loads to be transferred from the low-angle helical layers on the inside through the high-angle helical layers to the circumferential layers positioned on the laminate outside. This not only causes a generally higher cylinder expansion, but also increases the likelihood of developing interfiber failure in low-angle and high-angle helical layers. Evolving interfiber failure in the helical layers not only increases the overall component compliance (which is seen in Fig. 12, where the tangential strain at 105 MPa is of 0.2% higher compared to Sequence BC), but also increases the ply stresses in the load carrying circumferential layers. For higher internal pressures, this effect further worsens until the maximum longitudinal ply stresses in the circumferential or high-angle helical layers are exceeded and the vessel subsequently collapses. In case of Sequence BC, this effect is anticipated to be much less apparent due to its specific stacking sequence. The circumferential layers are located at the position of highest tangential loads on the inside, which they carry and therefore prevent the vessel from largely expanding in the tangential direction. The low-angle helical and high-angle layers are not required to transfer high loads and therefore it is expected that less interfiber failure is evolving in these layer types. This reduces the rate at which load needs to be re-distributed because of interfiber failure, which in turn reduces the longitudinal ply stresses in the circumferential and high-angle helical layers and leads to an overall higher cylinder strength compared to Sequence BL.

While the modeling approach was able to capture general trends in the deformation behavior of both sequences, the neglection of local variations in fiber volume fraction and the neglection of damage hinder to correctly predict trends concerning the burst pressure. Table 3 shows the comparison of predicted and experimental burst pressures for Sequence BL and BC. For both sequences, the burst pressure is underestimated which is counterintuitive given the fact that a first-ply-failure criterion in the longitudinal direction (Puck) was used for the prediction of burst without considering any material degradation. The burst pressure is underestimated by 17.7% for Sequence BC and 0.9% for Sequence BL. The main reason for the underestimation of cylinder strength is due to the aforementioned fact that the thickness was refined without locally increasing the fiber volume fraction, which effectively removes composite material in the FE model. The differences in the relative prediction accuracy for Sequences BL (−0.9%) and BC (−17.7%) are anticipated in the different impact that the progression of damage has for each stacking sequence. Nonetheless, without further investigation this aspect is hard to quantify by the time writing.

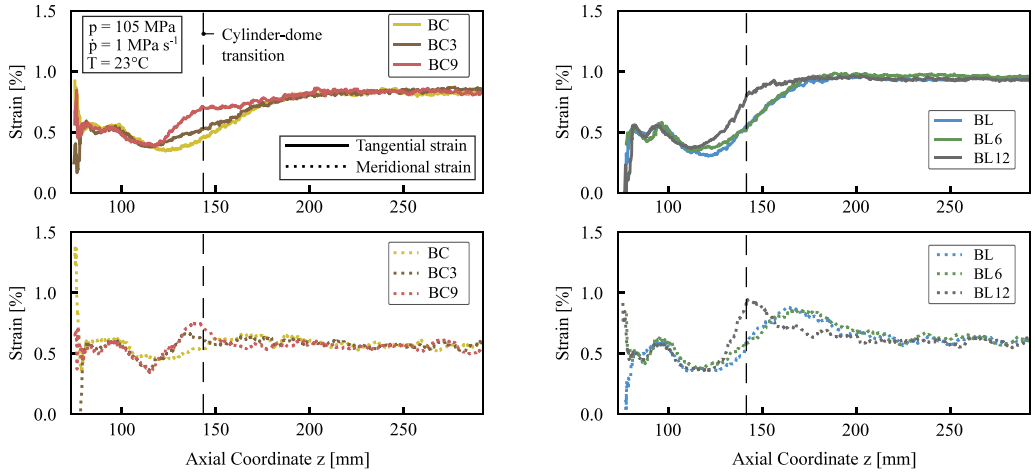

Fig. 14. Influence of the circumferential ply drop locations on the meridional and tangential strain components for Sequences BL, BL6, BL12, BC, BC3 and BC9.

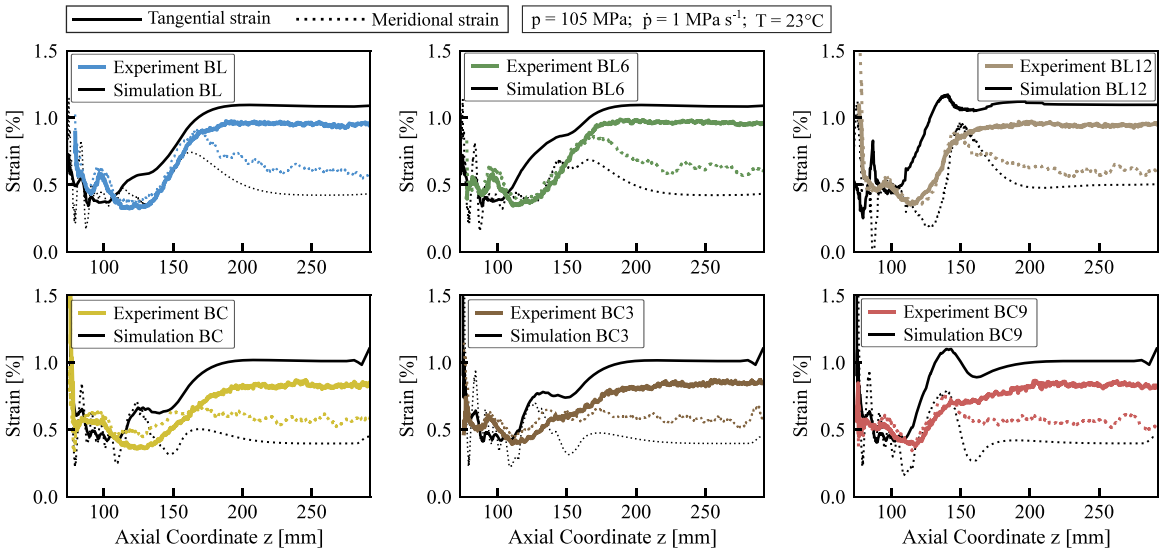

Fig. 15. Comparison of predicted and experimental strains along the meridional surface path for Sequences BL, BL6, BL12, BC, BC3 and BC9.

5.2. Variation of circumferential ply drop locations

After evaluating the influence of the stacking sequence, this section is aimed to access the influence of the circumferential ply drop locations. Therefore, all the configurations shown in Fig. 5 are considered to highlight the different impact that circumferential ply drop locations can have on the deformation behavior and on the final failure.

Impact on the strain distribution in the cylinder–dome transition

By varying the circumferential ply drop locations, the tangential stiffness distribution in the cylinder–dome transition is changed. Therefore it is expected that observable differences in the tangential strain distribution around the cylinder–dome transition will arise, that may also affect the meridional bending in this area to some extend. Fig. 14 shows the experimental strains in meridional and tangential direction for all BL and BC configurations. Expectedly, for all BL and BC configurations with retracted circumferential ply drop locations an increase in tangential strain at the transition is recognized. Depending on the magnitude of retraction and the stacking sequence, this effect is differently strong noticed. In case of the BL series, the retraction by 6 mm (BL6) only marginally increases the tangential strain distribution, whereas for a retraction by 12 mm (BL12) a more pronounced tangential expansion is recognized. Interestingly, the retraction of the circumferential ply drop locations not only causes an increase in outer surface meridional strain, but also shifts the position of where the maximum meridional strain is located, which is particularly visible when comparing the Sequences BL and BL12. The higher compliance in the tangential direction at the transition, not only increases the meridional bending of the cylinder end but also the position of where the cylinder is bending inwards shifts.

For the BC series, a higher sensitivity of the deformation behavior to the circumferential ply drop retraction seems to exist. When retracting the circumferential ply drop locations by only 3 mm (BC3) an increase in tangential strain is noticed in the transition. This is further amplified when retracting the ply drop locations by 9 mm (BC9) compared to the initial configuration (BC). Similar to the BL configurations, the missing tangential stiffness also increases and shifts the position of maximum outer meridional strain in the transition, as the comparison of Sequences BC9 and BC indicates.

Fig. 15 shows the comparison of predicted and experimental strains along the meridional surface path for all investigated sequences. While the general discrepancies hold true for all sequences (overestimation of tangential strains and underestimation of meridional strains), it becomes clear that the distinct responses of the sequences in the cylinder–dome transition region are well represented by the FE model. Particularly the configurations with maximum retraction of circumferential ply drop locations (BC9 and BL12) are captured very reasonably

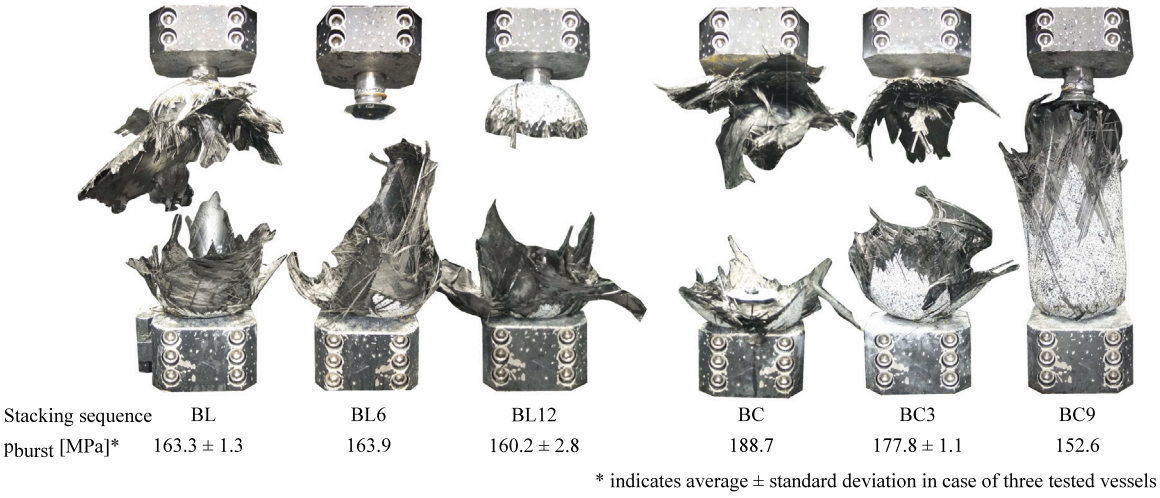

Fig. 16. Example of vessel remainder for each investigated sequence.

in terms of their local increases in meridional and tangential strains in the cylinder–dome transition region.

Influence on failure mode and burst pressure

The impact of retracting circumferential ply drop locations on the deformation behavior can be summarized as a local increase (and partial shift) in tangential and meridional strains in the cylinder–dome transition. While the observed trends in deformation behavior were reasonable and expected, the question arises whether the retraction in circumferential ply drop locations causes a noticeable change in the failure mode and/or decrease in burst pressure. To evaluate this aspect, the vessel remainder, the experimental burst pressures as well as the numerical predictions are considered.

Fig. 16 shows one vessel remainder per sequence and the corresponding obtained burst pressures. Based upon the remainders a different failure mode could be attributed to the Sequences BL6 and BC9. For both sequences, partial sections of the upper dome half are gone, while for the other configurations mainly the cylindrical section is missing. Nonetheless, as only one vessel for these configurations was tested, it is necessary to also consider the trends in burst pressure.

When evaluating the experimental burst pressures, it becomes clear that the impact of circumferential ply drop locations on the final burst pressure is highly dependent on the type of stacking sequence. For the BL series, a very minor decrease in burst pressure is noticed between BL, BL6 and BL12. In fact, the burst pressure is decreasing by 1.9% between the basic configuration (BL) and the configuration of highest circumferential ply drop retraction (BL12), which suggests that the retraction of circumferential ply drop locations neither majorly impacted the failure mode nor the burst pressures of the BL sequences. Contrarily, the obtained burst pressures for the BC series show a much higher sensitivity to the retraction of circumferential ply drop locations. While a retraction of 3 mm in the ply drop locations (BC3) already shows a decrease in burst pressure by 5.8%, a retraction by 9 mm (BC9) results in a relative decrease by 19.1% compared to the baseline configuration (BC). Linking this fact with the obtained vessel remainder of Sequence BC9 leads to the conclusion that the retraction of circumferential ply drop locations not only severely impacted the burst performance of the BC series but also led to a change in failure mode in case of Sequence BC9, where failure is located outside of the cylinder.

The differences in the sensitivity of burst performance to the retraction of circumferential ply drop locations is visualized in Fig. 17. The exact source of this behavior is difficult to pinpoint by the time writing but is likely dependent on a few key aspects that are vastly different between the BC and BL series. In general, the interfaces between helical and circumferential layers in the cylinder–dome transition are deemed

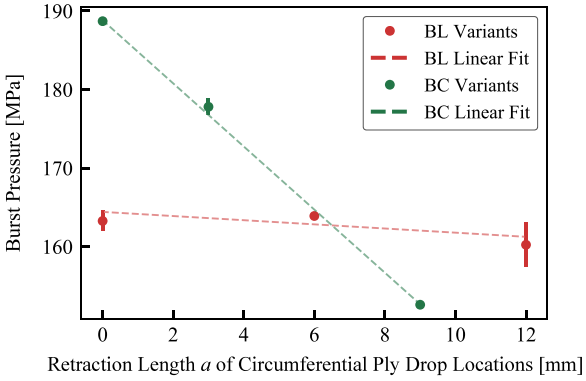

Fig. 17. Change in burst pressures as a function of the retraction length a of circumferential ply drop locations for the BL and BC series.

as critical interfaces, because of developing interlaminar stresses. As subsequent circumferential plies are dropped off, sudden changes in stiffness further amplify the criticality of this interface.

In case of the BL and BC configurations, the through-the-thickness position of the interface between the circumferential layer stack and the majority of helical layers varies. In case of the BL series, this interface corresponds to the bottom of the circumferential layer stack and the top of the helical layer group (low-angle and high-angle helical layers) beneath. As the vessel is internally loaded and expands in radial and axial direction, the tangentially compliant helical layers are pushed against the stiff circumferential layers, which effectively reduces the likelihood of experiencing peel-off stresses.

In the BC series, the interface between the majority of helical layers and the circumferential layer stack is located at the top of the circumferential stack and the bottom of the helical layer group above. Contrarily to the aforementioned case, when subjected to internal pressure the tangentially compliant helical layers are no longer pushed against the circumferential stack because of their location through-the-thickness. At the tip, where the last tangentially reinforcing circumferential layer is dropped off, the compliant helical layer group is exposed to the governing tangential loads which results in a larger deformation at that position. This manifests itself in peel-off stresses between the compliant helical layer group and the circumferential layer stack below. With increasing pressure, interlaminar damage is expected to grow which in turn causes a re-distribution of load and potentially a premature failure. While the preceding paragraphs may provide a potential explanation for the different sensitivity of the BL

Table 4
Overview of predicted and experimental burst pressures for all investigated sequences.

Stacking sequence	Number of vessels	Burst pressure [MPa]		Relative difference
		Experiment	Simulation	
BL	3	163.3 ± 1.3	161.8	−0.9%
BL6	1	163.9	161.9	−1.2%
BL12	3	160.2 ± 2.8	161.9	+1.1%
BC	1	188.7	155.2	−17.7%
BC3	3	177.8 ± 1.1	155.5	−12.5%
BC9	1	152.6	147.1	−3.6%

and BC configurations to the circumferential ply drop locations, further experimental and numerical work is needed to confidently assure the described effects.

Concerning the comparison of predicted and experimental burst pressures, Table 4 provides an overview for all tested sequences. The general tendency to underestimate the burst pressure remains for all sequences but for the Sequence BL12, where a slight overestimation by +1.1% is noticed. While the magnitude in terms of burst pressure is particularly off for the Sequences BC (−17.7%) and BC3 (−12.5%), it is worth mentioning that the modeling approach was capable of predicting the different impact the circumferential ply drop locations have on the BL and BC series, at least trend-wise. For the BL series, a nearly constant burst pressure (161.8 or 161.9 MPa) is predicted no matter what the retraction of circumferential ply drop location is. Contrarily, in case of the BC series, a decreased burst pressure is predicted for Sequence BC9 (147.1 MPa) compared to the baseline configuration BC (155.1 MPa). Nonetheless, additionally to the aforementioned limitations of the modeling approach, the particular case of retracting circumferential ply drop locations in the cylinder–dome transition may also require the implementation of cohesive interfaces between the layer groups. This in turn, may not only increase the prediction accuracy but would also deliver valuable insights about the development of interlaminar damage and its impact on the final failure.

6. Conclusions

In this work, the effect of stacking sequence and circumferential ply drop locations on the mechanical response of type IV composite pressure vessels subjected to internal pressure is investigated. Through a comprehensive experimental set, where the two variables are varied, the impact of each own and the interaction between the both is assessed. In addition to the experimental results, the investigation is complemented by a numerical modeling approach, which aims to enable an accurate prediction of deformation behavior and burst pressure for a variety of stacking sequences, while remaining computationally efficient. The main outcomes of this work can be briefly summarized in the following bulletpoints:

(i) The stacking sequence determines the stiffness distribution through-the-thickness and therefore greatly affects the cylinder expansion, particularly in the tangential direction. Depending on the magnitude of which the cylinder expands tangentially, the meridional bending at the cylinder–dome transition varies.
(ii) For the investigated sequences and under the premise that the circumferential ply drop locations are comparable, the placement of tangentially reinforcing layers (e.g. circumferential and high-angle helicals) as inner layers resulted in overall lower tangential cylinder expansion and higher burst pressures.
(iii) The retraction of circumferential ply drop locations not only leads to a local increase in tangential strain at the cylinder–dome transition, but also affects the magnitude and position of maximum outer meridional strain.
(iv) The impact of circumferential ply drop locations on the burst performance of type IV pressure vessels is greatly dependent on the stacking sequence. In this investigation, sequences with circumferential layers and high-angle helical layers positioned as inner layers (BC series) showed a high sensitivity to any ply drop retraction. Contrarily, for sequences with circumferential layers and high-angle helical layers as outer layers (BL series), a change in burst performance was barely noticeable even when retracting all circumferential ply drop locations by 12 mm. The reason for the difference in the sensitivity between the sequences is believed to be in the distinct layer interfaces and the development of interlaminar damage linked to it.

It is worthwhile to mention at this point, that the observed effects hold true for the investigated layup composition (ratio of circumferential, high-angle and low-angle helical layers). Any changes to the composition itself may lead to differences magnitude and/or trend-wise. For example, the sensitivity of the circumferential ply drop locations may not be as severe for a layup, which is barely composed of any circumferential layers. Therefore, extending the investigation on multiple differently composed layups will open up an interesting discussion in the future and in turn will allow more generic conclusions.

CRediT authorship contribution statement

M. Nebe: Project administration, Conceptualization, Methodology, Investigation, Validation, Visualization, Writing – original draft preparation. **A. Johman:** Data curation, Methodology, Software, Investigation, Validation, Writing – original draft preparation. **C. Braun:** Resources, Supervision, Writing – review & editing. **J.M.J.F. van Campen:** Supervision, Writing – review & editing.

Declaration of competing interest

The authors declare that they have no known competing financial interests or personal relationships that could have appeared to influence the work reported in this paper.

Acknowledgments

The authors would like to acknowledge all students that contributed to his research in the past years. These are Daniel Maraite, Ana Isabel Torres Guijarro, Tom Asijee, Benoît Porra, Eleonora Cesari, Alexander Kasses, Antonio Johman, Alejandro Soriano Sutil and Chiara Ardemani.

References

[1] O'Malley K, Ordaz G, Adams J, Randolph K, Ahn CC, Stetson NT. Applied hydrogen storage research and development: A perspective from the U.S. department of energy. J Alloys Compd 2015;645:419–22. http://dx.doi.org/10.1016/j.jallcom.2014.12.090.
[2] Ramirez JPB, Halm D, Grandidier J, Villalonga S, Nony F. 700 Bar type IV high pressure hydrogen storage vessel burst – simulation and experimental validation. Int J Hydrogen Energy 2015;40(38):13183–92. http://dx.doi.org/10.1016/j.ijhydene.2015.05.126.
[3] USDepartment of Energy. Annual Progress Report - DOE Hydrogen and Fuel Cells Program. DOE/GO-102013-4260 U.S. Department of Energy URL https://www.hydrogen.energy.gov/annual_progress13.html.
[4] Downs KS, Hamstad MA. Acoustic emission from depressurization to detect/evaluate significance of impact damage to graphite/epoxy pressure vessels. J Compos Mater 1998;(32):258–307.

[5] Chou HY, Mouritz AP, Bannister MK, Bunsell AR. Acoustic emission analysis of composite pressure vessels under constant and cyclic pressure. Composites A 2015;70:111–20. http://dx.doi.org/10.1016/j.compositesa.2014.11.027.
[6] Sause MGR, Schmitt S, Hoeck B, Monden A. Acoustic emission based prediction of local stress exposure. Compos Sci Technol 2019;173:90–8. http://dx.doi.org/10.1016/j.compscitech.2019.02.004.
[7] Yao XF, Meng LB, Jin JC, Yeh HY. Full-field deformation measurement of fiber composite pressure vessel using digital speckle correlation method. Polym Test 2005;24(2):245–51. http://dx.doi.org/10.1016/j.polymertesting.2004.05.009.
[8] Meng LB, Jin GC, Yao XF, Yeh HY. 3D full-field deformation monitoring of fiber composite pressure vessel using 3D digital speckle correlation method. Polym Test 2006. http://dx.doi.org/10.1016/j.polymertesting.2005.09.011.
[9] Hao J-C, Leng J-S, Wei Z. Non-destructive evaluation of composite pressure vessel by using FBG sensors. Chin J Aeronaut 2007;20(2):120–3. http://dx.doi.org/10.1016/S1000-9361(07)60017-X.
[10] Leh D, Saffré P, Francescato P, Arrieux R, Villalonga S. A progressive failure analysis of a 700-bar type IV hydrogen composite pressure vessel. Int J Hydrogen Energy 2015;40(38):13206–14. http://dx.doi.org/10.1016/j.ijhydene.2015.05.061.
[11] Degrieck J, de Waele W, Verleysen P. Monitoring of fibre reinforced composites with embedded optical fibre bragg sensors, with application to filament wound pressure vessels. NDT E Int 2001;34(4):289–96. http://dx.doi.org/10.1016/S0963-8695(00)00069-4.
[12] Tapeinos IG, Rajabzadeh A, Zarouchas DS, Stief M, Groves RM, Koussios S, et al. Evaluation of the mechanical performance of a composite multi-cell tank for cryogenic storage: Part II – experimental assessment. Int J Hydrogen Energy 2019;44(7):3931–43. http://dx.doi.org/10.1016/j.ijhydene.2018.12.063.
[13] Gasior P, Malesa M, Kaleta J, Kujawińska M, Malowany K, Rybczyński R. Application of complementary optical methods for strain investigation in composite high pressure vessel. Compos Struct 2018;203:718–24. http://dx.doi.org/10.1016/j.compstruct.2018.07.060.
[14] Nebe M, Asijee TJ, Braun C, van Campen JMJF, Walther F. Experimental and analytical analysis on the stacking sequence of composite pressure vessels. Compos Struct 2020. http://dx.doi.org/10.1016/j.compstruct.2020.112429.
[15] Nebe M, Soriano A, Braun C, Middendorf P, Walther F. Analysis on the internal pressure loading of composite pressure vessels: FE modeling and experimental correlation. Compos B 2021. http://dx.doi.org/10.1016/j.compositesb.2020.108550.
[16] Leh D, Magneville B, Saffré P, Francescato P, Arrieux R, Villalonga S. Optimisation of 700 bar type IV hydrogen pressure vessel considering composite damage and dome multi-sequencing. Int J Hydrogen Energy 2015;40(38):13215–30. http://dx.doi.org/10.1016/j.ijhydene.2015.06.156.
[17] Roh HS, Hua TQ, Ahluwalia RK. Optimization of carbon fiber usage in type 4 hydrogen storage tanks for fuel cell automobiles. Int J Hydrogen Energy 2013;38(29):12795–802. http://dx.doi.org/10.1016/j.ijhydene.2013.07.016.
[18] Wang L, Zheng C, Luo H, Wei S, Wei Z. Continuum damage modeling and progressive failure analysis of carbon fiber/epoxy composite pressure vessel. Compos Struct 2015;134:475–82. http://dx.doi.org/10.1016/j.compstruct.2015.08.107.
[19] Son D, Chang SH. Evaluation of modeling techniques for a type III hydrogen pressure vessel (70 MPa) made of an aluminum liner and a thick carbon/epoxy composite for fuel cell vehicles. Int J Hydrogen Energy 2012;37(3):2353–69. http://dx.doi.org/10.1016/j.ijhydene.2011.11.001.
[20] Zu L, Xu H, Wang H, Zhang B, Zi B. Design and analysis of filament-wound composite pressure vessels based on non-geodesic winding. Compos Struct 2019;207:41–52. http://dx.doi.org/10.1016/j.compstruct.2018.09.007.
[21] Zhang Q, Xu H, Jia X, Zu L, Cheng S, Wang H. Design of a 70 MPa type IV hydrogen storage vessel using accurate modeling techniques for dome thickness prediction. Compos Struct 2020;236:111915. http://dx.doi.org/10.1016/j.compstruct.2020.111915.
[22] Liu PF, Chu JK, Hou SJ, Zheng JY. Micromechanical damage modeling and multiscale progressive failure analysis of composite pressure vessel. Comput Mater Sci 2012;60:137–48. http://dx.doi.org/10.1016/j.commatsci.2012.03.015.
[23] Wang L, Zheng C, Wei S, Wei Z. Micromechanics-based progressive failure analysis of carbon fiber/epoxy composite vessel under combined internal pressure and thermomechanical loading. Composites B 2016;89:77–84. http://dx.doi.org/10.1016/j.compositesb.2015.11.018.
[24] Leone FA, Bergan AC, Dávila CG. Compdam - deformation gradient decomposition (DGD), v2.5.0. 2019, https://github.com/nasa/CompDam_DGD.
[25] Nebe M. In situ characterization methodology for the design and analysis of composite pressure vessels. Wiesbaden: Springer Vieweg Verlag; 2022, http://dx.doi.org/10.1007/978-3-658-35797-9.
[26] Xia M, Takayanagi H, Kemmochi K. Analysis of multi-layered filament-wound composite pipes under internal pressure. Compos Struct 2001;53(4):483–91. http://dx.doi.org/10.1016/S0263-8223(01)00061-7.
[27] ISO 527-4:1997. Plastics - determination of tensile properties - part 4: test conditions for isotropic and orthotropic fibre-reinforced plastic composites. ISO/TC 61/SC 13 Composites and Reinforcement Fibres; 1997.
[28] ISO 14129:1997. Fibre-reinforced plastic composites - determination of the in-plane shear stress/shear strain response, including the in-plane shear modulus and strength, by the plus or minus 45 degree tension test method. ISO/TC 61/SC 13 Composites and Reinforcement Fibres; 1997.
[29] DIN EN 2564:2019-08. Aerospace series - carbon fibre laminates - determination of the fibre, resin and void contents; German and English version EN 2564:2018. Berlin, Germany: Deutsches Institut für Normung; 2019, http://dx.doi.org/10.1520/D6671_D6671M-19.
[30] ComposiCAD documentation. ComposiCAD; 2020.
[31] Johman A. Development of a computationally efficient analysis framework for type IV pressure vessels. (MSc Thesis), Delft University of Technology; 2021.
[32] Kang C, Shi Y, Deng B, Yu T, Sun P. Determination of residual stress and design of process parameters for composite cylinder in filament winding. Adv Mater Sci Eng 2018;2018(1):1–11. http://dx.doi.org/10.1155/2018/1821342.
[33] Rafiee R, Torabi M. Stochastic prediction of burst pressure in composite pressure vessels. Compos Struct 2018;185:573–83. http://dx.doi.org/10.1016/j.compstruct.2017.11.068.